THE JOURNAL OF PHYSICAL CHEMISTRY Letters

Letter

pubs.acs.org/JPCL

# Bilayer Deformation, Pores, and Micellation Induced by Oxidized Lipids

Phansiri Boonnoy,[†] Viwan Jarerattanachat,[†,‡] Mikko Karttunen,[*,§] and Jirasak Wong-ekkabut[*,†]

[†]Department of Physics, Faculty of Science, Kasetsart University, Bangkok, 10900, Thailand

[‡]Clarendon Laboratory, Department of Physics, University of Oxford, Oxford OX1 3PU, United Kingdom

[§]Department of Mathematics and Computer Science & Institute for Complex Molecular Systems, Eindhoven University of Technology, MetaForum, 5600 MB Eindhoven, The Netherlands

Supporting Information

**ABSTRACT:** The influence of different oxidized lipids on lipid bilayers was investigated with 16 individual 1 $\mu$s atomistic molecular dynamics (MD) simulations. Binary mixtures of lipid bilayers of 1-palmitoyl-2-linoleoyl-*sn*-glycero-3-phosphatidylcholine (PLPC) and its peroxide and aldehyde products were performed at different concentrations. In addition, an asymmetrical short chain lipid, 1-palmitoyl-2-decanoyl-*sn*-glycero-3-phosphatidylcholine (PDPC), was used to compare the effects of polar/apolar groups in the lipid tail on lipid bilayer. Although water defects occurred with both aldehyde and peroxide lipids, full pore formation was observed only for aldehyde lipids. At medium concentrations the pores were stable. At higher concentrations, however, the pores became unstable and micellation occurred. Data analysis shows that aldehyde lipids' propensity for pore formation is due to their shorter and highly mobile tail. The highly polar peroxide lipids are stabilized by strong hydrogen bonds with interfacial water.

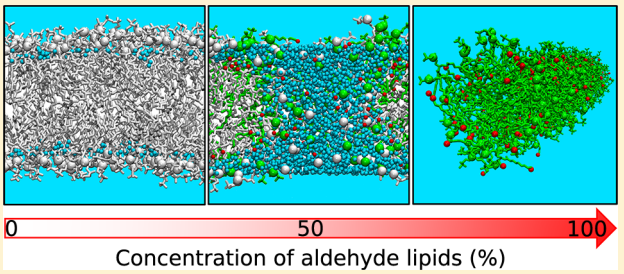


Lipid peroxidation results from oxidative attack on the unsaturated lipid acyl chains by free radicals ($OH^-$, $O_2^-$, etc.).[1] Two major oxidized species are typically produced: hydroxyl- or hydroperoxy-dieonyl and truncated chains with an aldehyde or carboxylic group.[2] Oxidized lipids have polar moieties at their terminals,[3] and they can strongly modify membrane structures and their biological functions.[4−6] The oxidized lipid chain reversal is considered as the main cause of such changes.[7−12] Consequences include increased area per lipid, bilayer thinning, decrease of lipid tail order parameter, and variations in the lateral diffusion coefficient.[2,10−14] These changes due to oxidized lipids have been observed to cause an increase in water permeability and to lead to membrane deformation.[15,16]

Previous free energy calculations have suggested that oxidized lipids with a hydroperoxide functional group have more potential to disturb the bilayer than the ones with an aldehyde group.[11] In contrast, Cwiklik et al.[17] and Lis et al.[13] used MD simulations and found that massive aldehyde oxidation lead to pore creation and bilayer deformation. However, because of the limited number of studies and limitations in simulation times, pore formation caused by lipid peroxidation remains unresolved. Recently, Villanueva et al.[18] demonstrated passive pore formation in ester-modified lipid bilayer mixtures and described the possibility of pore creation by hydroperoxy-dieonyl lipids. This has not been directly observed, although permeability of water has been predicted to be higher than when aldehyde lipids are present.[11]

Here, over 16 $\mu$s MD simulations of binary mixture lipid bilayers of 1-palmitoyl-2-linoleoyl-*sn*-glycero-3-phosphatidylcholine (PLPC) and its four major oxidative products[19−21] including two hydroperoxides (1-palmitoyl-2-(9-hydroperoxy-trans-10, cis-12-octadecadienoyl)-*sn*-glycero-3-phosphocholine, 9-tc and 1-palmitoyl-2-(13-hydroperoxy-trans-11, cis-9-octadecadienoyl)-*sn*-glycero-3-phosphocholine, 13-tc), and two aldehydes (1-palmitoyl-2-(9-oxo-nonanoyl)-*sn*-glycero-3-phosphocholine, 9-al and 1-stearoyl-2-(12-oxo-cis-9-dodecenoyl)-*sn*-glycero-3-phosphocholine, 12-al) were carried out at concentrations of 50, 75, and 100%. The structures of different lipids are shown in Supporting Information Figure S1. In addition, the 1-palmitoyl-2-decanoyl-*sn*-glycero-3-phosphatidylcholine (PDPC), the oxidized derivative of PLPC with a truncated and nonpolar *sn*-2 chain, was used to investigate the effects of asymmetric lipid tail length on bilayer properties. We observed that oxidized lipids with an aldehyde functional group disturb the bilayer more than the ones with a peroxide group. We show, however, that previous simulations did not probe long enough time scales: Slow dynamics of self-assembly and restructuring requires much longer simulation times. The results show how the polar groups perturb the bilayers and induce pore formation, bilayer deformation, and even micelle formation.

**Received:** October 27, 2015
**Accepted:** November 24, 2015





DOI: 10.1021/acs.jpclett.5b02405
*J. Phys. Chem. Lett.* 2015, 6, 4884−4888

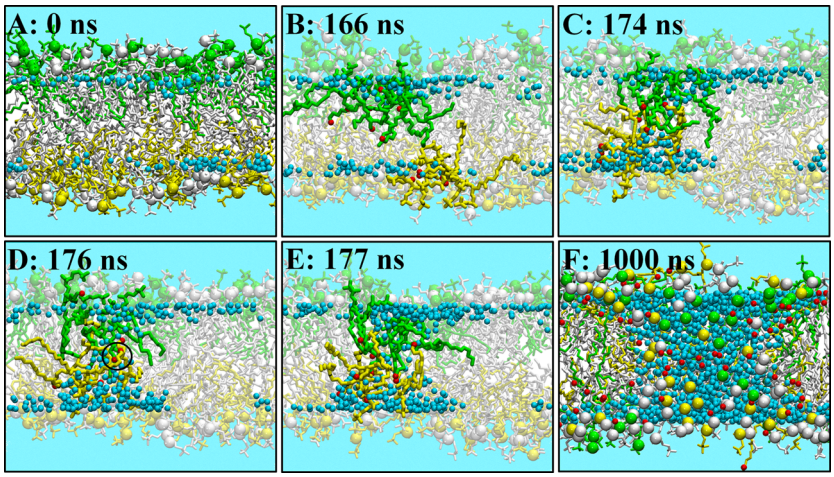


**Figure 1.** Pore formation in the 50% 9-al system. Initially, the oxidized lipids were randomly distributed in the bilayer (A). Aggregation (B) followed by formation of water defects (C); water is pulled into the bilayer by the aldehyde groups. Then, oxidized lipids from the two leaflets reach contact (D) leading to the formation of a water bridge (E). The bridge extends to form a stable pore (F). Green and yellow: 9-al lipids in the upper and lower leaflets, respectively. White: PLPC. Green, yellow and white spheres: Phosphorus atoms on the different lipids. Red spheres: Oxygens in 9-al *sn*-2 tails. Blue: water.

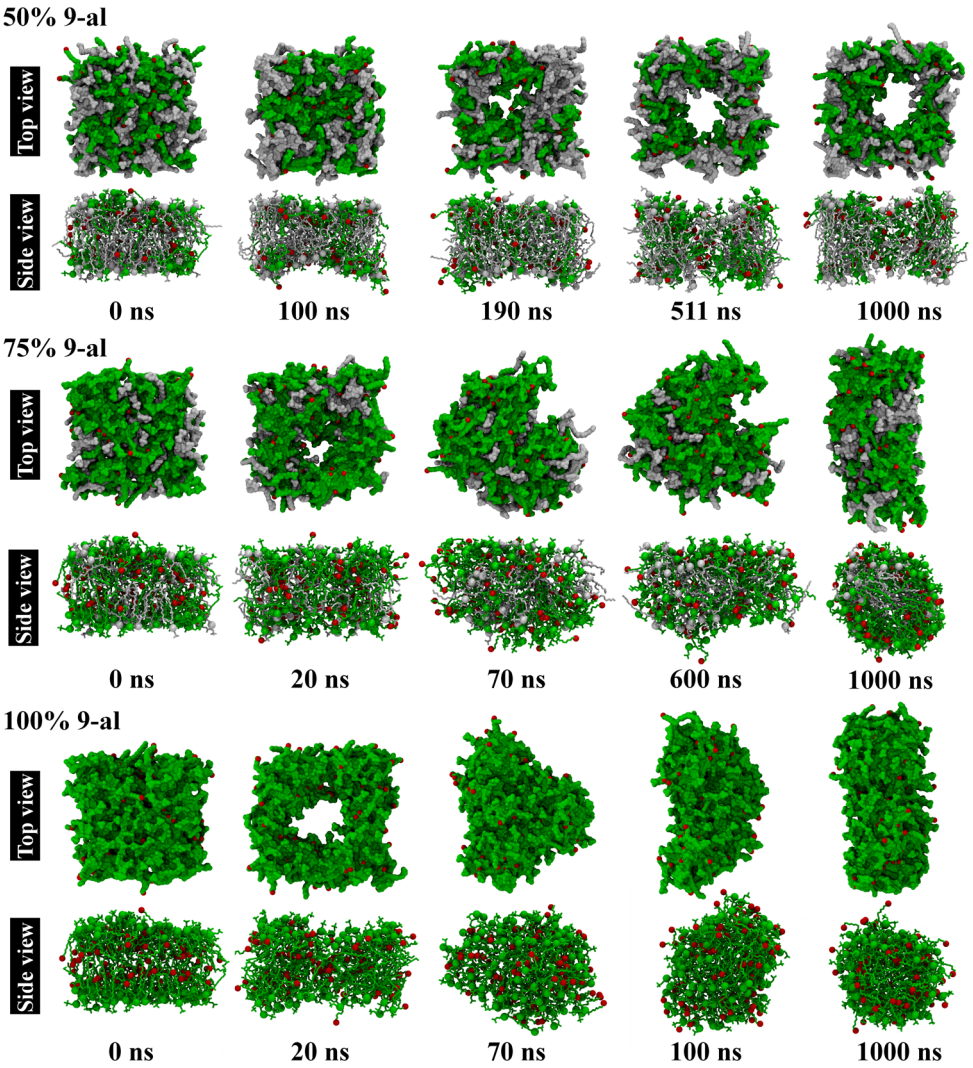


**Figure 2.** Time evolution of PLPC and 9-al mixtures at 50%, 75%, and 100% of 9-al. Water molecules are not shown for clarity. White and green: PLPC and 9-al molecules, respectively. Red: Oxygen atoms in aldehyde groups.



DOI: 10.1021/acs.jpclett.5b02405
*J. Phys. Chem. Lett.* 2015, 6, 4884−4888

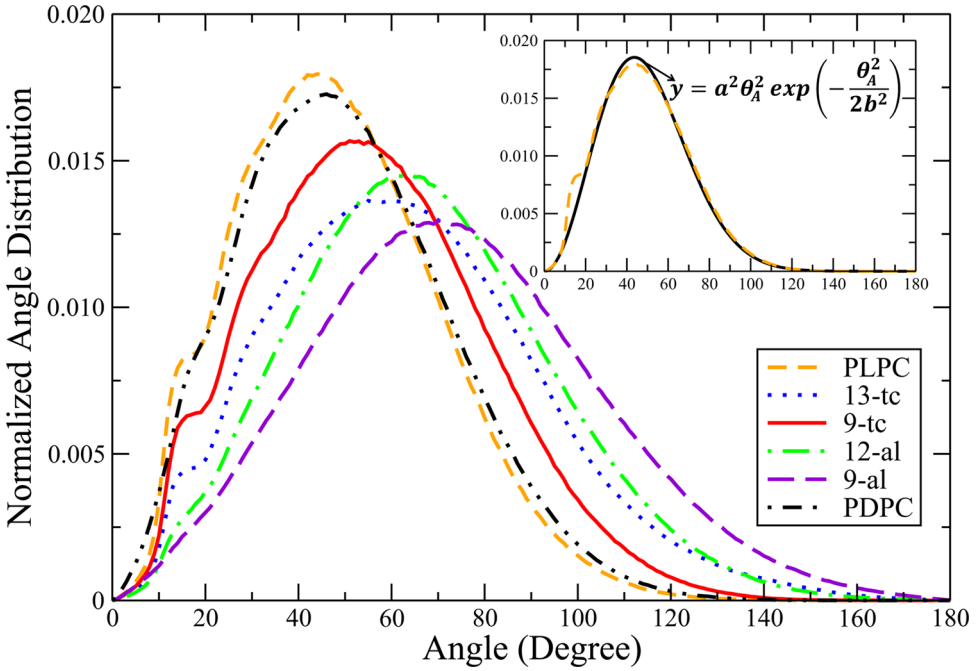


**Figure 3.** Distribution of $\theta_A$ for pure PLPC and oxidized lipids. Inset shows the fit of $\theta_A$ for pure PLPC lipid using the Boltzmann distribution.

All simulations had 128 lipids and 10 628 simple point charge (SPC) waters.[22] PLPC and oxidized lipid topologies were taken from previous studies and described by the same united-atom force field.[11,12,23] The binary mixtures were prepared by replacing the linoleate chains in PLPC lipids[11,12] with 9-tc, 13-tc, 9-al, 12-al, and caprylic acid in amounts of 64, 96, and 128 molecules (concentrations of 50, 75, and 100%). The oxidized lipids were randomly distributed with equal number in both leaflets. The simulated systems are listed in Table S1. After energy minimization using steepest descents, atomistic MD simulations were run for 1 $\mu$s with 2 fs time step by using GROMACS 4.5.5.[24,25] Periodic boundary conditions were applied. A 1.0 nm cutoff was used for the Lennard-Jones interactions and the real part of the electrostatic interactions, and the neighbor list was updated at every time step to minimize artifacts.[26,27] The particle−mesh Ewald method[28] was used for electrostatics, and bond lengths were constrained by the LINCS algorithm.[29] Temperature was set to 298 K using the v-rescale algorithm.[30] The Berendsen barostat[31] (1 bar) with a time constant of 4.0 ps and compressibility of $4.5 \times 10^{-5}$ $bar^{-1}$ was used. Visual Molecular Dynamics software was used for visualizations.[32]

Oxidized lipids can facilitate damage on a membrane. Such induced damage may come in the form of water defects that are local clusters causing significant local bilayer disorder and water conducting pores. Pores are particularly significant since water can permeate through the bilayer with permeability of about 2 orders of magnitude higher than via spontaneous translocation through a bilayer with no pore.[13] Next, we investigate the different mechanisms causing damage.

Increasing concentration of lipids with polar tails (13-tc, 9-tc, 12-al and 9-al) led to an increase in the area per lipid and a decrease in bilayer thickness, as shown in Table S2. This is in agreement with previous studies.[11,12,33] With oxidized lipids with truncated and apolar tails (PDPC), the area/lipid decreased only slightly (see Table S2), but the bilayer thickness decreased significantly with increasing concentration. Interestingly, with PDPC the thicknesses are very close to 9-tc at all concentrations. This suggests that the length of the hydrocarbon chain after the last oxygen in hydrocarbon chain (there are 10 carbons after the last oxygen in chain for both PDPC and 9-tc lipids) has a significant influence on bilayer thickness but only a small effect on the area/lipid.[34] Changes in area/lipid and thickness have been suggested to be important factors in pore formation with oxidized lipids present.[13,35] However, we observed no pores in the 100% 13-tc bilayer, even though it has larger area per lipid and is thinner than the 50% aldehyde mixture in which pores occurred. This implies that large area per lipid and small thickness are not the only contributing factors when oxidized lipids are present. The change in volume per lipid was considered for truncated (aldehyde lipids and PDPC) and nontruncated lipids (PLPC and peroxide lipids). With truncated tails (12-al, 9-al, and PDPC), the volume per lipid decreased markedly in contrast to the peroxide lipids for which only a small change was observed.

Water defects occurred in all systems with polar tails (13-tc, 9-tc, 12-al, and 9-al). Full pore formation was observed with aldehyde mixtures within a few hundred nanoseconds, but it was absent in the peroxide systems, even beyond times of 1 $\mu$s. This appears to contradict our previous study,[11] which suggested that peroxide lipids might be the most potent in inducing pore formation because of high water permeability. Although extensive at the time, the earlier simulations were run only for 180 ns. Figure 1 shows pore formation in the 50% 9-al system: (1) Aggregation of oxidized lipids is followed by formation of water defects in which water molecules are pulled into the bilayer by the aldehyde groups (Figure 1A,B). (2) The number of contacts between the aldehyde lipids belonging to the opposite sides of the bilayer increases, leading to a decrease in bilayer thickness (Table S2). (3) The oxygens in the aldehyde groups access the water interface of the opposing leaflets, allowing water to enter the bilayer interior (Figure 1C,D). (4) Waters form a bridge across the bilayer and create an unstable pore (Figures 1E). (5) Finally, the lipids at the



DOI: 10.1021/acs.jpclett.5b02405
J. Phys. Chem. Lett. 2015, 6, 4884−4888

edges of the water bridge flip and orient their head groups toward water to stabilize the pore (Figures 1F). For 75% 9-al, and 100% 9-al and 12-al mixtures, the pores were unstable and the bilayers deformed into stable rod-like micelles (Figure 2). Further snapshots are shown in Figure S2. The final structures after 1 $\mu$s are summarized in Table S1.

Neither pores nor micelles were observed for the peroxide lipid mixtures, in agreement with the experimental evidence as reported by Weber et al.[33] One possible explanation is that since the peroxide groups are highly polar, they are able to form strong hydrogen bonds with water molecules enabling them to stay at the interface.[11] Aldehyde lipid tails, however, are significantly more mobile than the peroxide ones as seen from the time evolution of the oxidized groups (Figure S3). This is also observable in the snapshots from different times along the trajectory which show that the aldehyde lipid tails pull water across the bilayer as shown in Figure S4.

To understand the structures, the shapes of individual lipid were analyzed. First, the distances between the headgroup phosphates and the last atoms of the *sn*-1 and *sn*-2 chains were calculated to characterize the tail lengths. They are denoted as $l_1$ and $l_2$, respectively. In addition, to characterize the separation between the *sn*-1 and *sn*-2 chains, the distance between their last atoms, $l_3$, was calculated. Finally, to characterize lipid geometry, the interior angles $\theta_A$, $\theta_B$, and $\theta_C$ were calculated. The tilt angle ($\theta_N$) between the *sn*-1 and the bilayer normal was used to determine lipid orientation. The definitions of $l_1$, $l_2$, $l_3$, $\theta_A$, $\theta_B$, $\theta_C$, and $\theta_N$ are shown in Figure S5.

The average angles $\langle\theta_A\rangle$, $\langle\theta_B\rangle$, $\langle\theta_C\rangle$, and $\langle\theta_N\rangle$ are summarized in Table S3. The average angles $\langle\theta_A\rangle$ of PLPC, 13-tc, 9-tc, 12-al, 9-al and PDPC are 48 ± 1$^o$, 63 ± 1$^o$, 56 ± 2$^o$, 67 ± 2$^o$, 74 ± 2$^o$, and 50 ± 1$^o$, respectively. The angles for lipids with polar tails are significantly larger than the ones with apolar tails. The tilt angle $\langle\theta_N\rangle$ of PLPC is approximately 30 ± 1$^o$ and significantly smaller than that of oxidized lipids ($\langle\theta_N\rangle$ of 13tc, 9tc, and PDPC are 36 ± 1$^o$, 33 ± 1$^o$, and 32 ± 1$^o$, respectively.). Previous studies[11,12] have suggested that the strong hydrogen bonds of the peroxide functional groups with water molecules are a result of the peroxide functional group staying at the lipid−water interface, while the aldehyde functional group penetrates deeply inside the bilayer. An increase in $\theta_A$ and $\theta_N$ corresponds to an increase in the area per lipid for polar oxidized lipid. Considering the distribution of $\theta_A$ (Figure 3), the means and variances of $\theta_A$ were calculated by fitting with the Boltzmann distribution as shown in Table S4. The variances of $\theta_A$ suggest that the aldehyde functional group distribution is wider than the peroxide one. This is in agreement with the electron density distribution of functional groups in oxidized lipids[11] and the *sn*-2 tilt angle distributions.[12]

The results in Table S5 show that $l_1$ are the same for all lipids, and $l_2$ of the truncated lipids (12-al, 9-al, PDPC) are significantly smaller than others. The ratios $l_1$:$l_2$ are close to 1 for the nontruncated lipids (PLPC and peroxide) and greater than 1 for the truncated lipids. For PLPC, peroxide lipids, and PDPC, the ratios of $l_2$:$l_3$ are close to or greater than 1, but for the aldehyde lipids they are significantly smaller than 1: for 12-al and 9-al, $l_2$:$l_3$ are 0.78 and 0.65, respectively.

The average geometries of the lipids and the self-assembled structures are shown in Figure S6. The typical shapes of PLPC, PDPC, and peroxide lipids are cylindrical with differences in their cross-sectional areas and heights. These two factors are directly related to the area per lipid and bilayer thickness. The conical shapes of the truncated oxidized lipids, especially polar aldehyde lipids, can induce positive membrane curvature[36] and partial interdigitation,[37] leading to pore formation.[38] Our results confirm this.

The packing parameter, $S = v_c/al_c$, is a concept to estimate aggregate morphologies based on lipid geometries.[39] $v_c$ is the average volume of the hydrocarbon chain, $a$ is the average surface area of the lipid headgroup, and $l_c$ is the average hydrocarbon chain length. The pure PLPC and the pure oxidized lipid systems were analyzed in terms of the packing parameter. The results are shown in Table S6. Based on the packing parameter, PLPC, 13-tc, 9-tc, and PDPC lipids can be characterized as cylindrical ($S \sim 1$). Thus, the equilibrium aggregate structures are bilayers. In the case of 12-al and 9-al lipids, the geometry is a truncated cone ($S \sim 0.5$). This predicts a micellar aggregate.

In conclusion, the disturbances induced by oxidized lipids on bilayers were studied by 16 $\mu$s MD simulations using bilayers consisting of binary mixtures of PLPC and its oxidative products at high concentrations. Our results show that, depending on aldehyde lipid concentration, stable or unstable pores are formed. Unstable pores, present at high concentrations, evolve into micelles. No pores were observed when peroxide lipids were present. Inside a pore, the polar groups distribute inside the bilayer and form a web-like structure in the order to induce water penetration. From analyzing the lipid geometries, we determined that the peroxide functional groups prefer to stay at the lipid−water interface rather than distribute inside the bilayer.[11] For the aldehyde lipids, the functional polar groups are highly mobile inside the bilayer (Figure S3) and can get into contact with other lipids in the opposing leaflet (Figure 1D). This is why pore formation occurs in aldehyde-containing bilayers and not when peroxide lipids are present. Our findings suggest that one of the key mechanisms for passive pore formation is the distribution of polar groups inside the bilayer. Micelle formation was observed in the systems of aldehyde lipids at high concentrations. Analysis of the lipid geometry suggests that the lipid shape plays an essential role in the self-assembly of lipid structures.

## ■ ASSOCIATED CONTENT

### Supporting Information

The Supporting Information is available free of charge on the ACS Publications website at DOI: 10.1021/acs.jpclett.5b02405.

Additional figures and tables as described in the text (PDF)

## ■ AUTHOR INFORMATION


### Corresponding Authors

*E-mail: jirasak.w@ku.ac.th (J.W.)

*E-mail: mkarttu@tue.nl (M.K.)


### Notes

The authors declare no competing financial interest.

## ■ ACKNOWLEDGMENTS

Financial support by Kasetsart University Research & Development Institute (KURDI; J.W.) and Faculty of Science (P.B. and J.W.) at Kasetsart University.

## ■ REFERENCES

(1) Brodnitz, M. H.; Nawar, W. W.; Fagerson, I. S. Autoxidation of Saturated Fatty Acids. I. The Initial Products of Autoxidation of Methyl Palmitate. *Lipids* **1968**, *3*, 59−64.



DOI: 10.1021/acs.jpclett.5b02405
*J. Phys. Chem. Lett.* 2015, 6, 4884−4888

(2) Jurkiewicz, P.; Olzynska, A.; Cwiklik, L.; Conte, E.; Jungwirth, P.; Megli, F. M.; Hof, M. Biophysics of Lipid Bilayers Containing Oxidatively Modified Phospholipids: Insights from Fluorescence and EPR Experiments and from MD Simulations. *Biochim. Biophys. Acta, Biomembr.* **2012**, *1818*, 2388−2402.
(3) Fruhwirth, G. O.; Loidl, A.; Hermetter, A. Oxidized Phospholipids: From Molecular Properties to Disease. *Biochim. Biophys. Acta, Mol. Basis Dis.* **2007**, *1772*, 718−736.
(4) Mandal, T. K.; Chatterjee, S. N. Ultraviolet- and Sunlight-Induced Lipid Peroxidation in Liposomal Membrane. *Radiat. Res.* **1980**, *83*, 290−302.
(5) Kunimoto, M.; Inoue, K.; Nojima, S. Effect of Ferrous Ion and Ascorbate-Induced Lipid Peroxidation on Liposomal Membranes. *Biochim. Biophys. Acta, Biomembr.* **1981**, *646*, 169−178.
(6) Nakazawa, T.; Nagatsuka, S.; Yukawa, O. Effects of Membrane Stabilizing Agents and Radiation on Liposomal Membranes. *Drugs Exp. Clin. Res.* **1986**, *12*, 831−835.
(7) Li, X. M.; Salomon, R. G.; Qin, J.; Hazen, S. L. Conformation of an Endogenous Ligand in a Membrane Bilayer for the Macrophage Scavenger Receptor CD36. *Biochemistry* **2007**, *46*, 5009−5017.
(8) Sabatini, K.; Mattila, J. P.; Megli, F. M.; Kinnunen, P. K. J. Characterization of Two Oxidatively Modified Phospholipids in Mixed Monolayers with DPPC. *Biophys. J.* **2006**, *90*, 4488−4499.
(9) Beranova, L.; Cwiklik, L.; Jurkiewicz, P.; Hof, M.; Jungwirth, P. Oxidation Changes Physical Properties of Phospholipid Bilayers: Fluorescence Spectroscopy and Molecular Simulations. *Langmuir* **2010**, *26*, 6140−6144.
(10) Khandelia, H.; Mouritsen, O. G. Lipid Gymnastics: Evidence of Complete Acyl Chain Reversal in Oxidized Phospholipids from Molecular Simulations. *Biophys. J.* **2009**, *96*, 2734−2743.
(11) Wong-ekkabut, J.; Xu, Z.; Triampo, W.; Tang, I. M.; Peter Tieleman, D.; Monticelli, L. Effect of Lipid Peroxidation on the Properties of Lipid Bilayers: A Molecular Dynamics Study. *Biophys. J.* **2007**, *93*, 4225−4236.
(12) Jarerattanachat, V.; Karttunen, M.; Wong-ekkabut, J. Molecular Dynamics Study of Oxidized Lipid Bilayers in NaCl Solution. *J. Phys. Chem. B* **2013**, *117*, 8490−8501.
(13) Lis, M.; Wizert, A.; Przybylo, M.; Langner, M.; Swiatek, J.; Jungwirth, P.; Cwiklik, L. The Effect of Lipid Oxidation on the Water Permeability of Phospholipids Bilayers. *Phys. Chem. Chem. Phys.* **2011**, *13*, 17555−17563.
(14) Plochberger, B.; Stockner, T.; Chiantia, S.; Brameshuber, M.; Weghuber, J.; Hermetter, A.; Schwille, P.; Schutz, G. J. Cholesterol Slows Down the Lateral Mobility of an Oxidized Phospholipid in a Supported Lipid Bilayer. *Langmuir* **2010**, *26*, 17322−17329.
(15) Sankhagowit, S.; Wu, S. H.; Biswas, R.; Riche, C. T.; Povinelli, M. L.; Malmstadt, N. The Dynamics of Giant Unilamellar Vesicle Oxidation Probed by Morphological Transitions. *Biochim. Biophys. Acta, Biomembr.* **2014**, *1838*, 2615−2624.
(16) Runas, K. A.; Malmstadt, N. Low Levels of Lipid Oxidation Radically Increase the Passive Permeability of Lipid Bilayers. *Soft Matter* **2015**, *11*, 499−505.
(17) Cwiklik, L.; Jungwirth, P. Massive Oxidation of Phospholipid Membranes Leads to Pore Creation and Bilayer Disintegration. *Chem. Phys. Lett.* **2010**, *486*, 99−103.
(18) Villanueva, D. Y.; Lim, J. B.; Klauda, J. B. Influence of Ester-Modified Lipids on Bilayer Structure. *Langmuir* **2013**, *29*, 14196−14203.
(19) Spiteller, P.; Kern, W.; Reiner, J.; Spiteller, G. Aldehydic Lipid Peroxidation Products Derived from Linoleic Acid. *Biochim. Biophys. Acta, Mol. Cell Biol. Lipids* **2001**, *1531*, 188−208.
(20) Pratt, D. A.; Mills, J. H.; Porter, N. A. Theoretical Calculations of Carbon-Oxygen Bond Dissociation Enthalpies of Peroxyl Radicals Formed in the Autoxidation of Lipids. *J. Am. Chem. Soc.* **2003**, *125*, 5801−5810.
(21) Porter, N. A.; Wujek, D. G. Autoxidation of Polyunsaturated Fatty Acids, an Expanded Mechanistic Study. *J. Am. Chem. Soc.* **1984**, *106*, 2626−2629.
(22) Berendsen, H. J. C.; Postma, J. P. M.; van Gunsteren, W. F.; Hermans, J. Interaction Models for Water in Relation to Protein Hydration. In *Intermolecular Forces*, Pullman, B., Ed.; D. Reidel: Dordrecht, The Netherlands, 1981; pp 331−342.
(23) Bachar, M.; Brunelle, P.; Tieleman, D. P.; Rauk, A. Molecular Dynamics Simulation of a Polyunsaturated Lipid Bilayer Susceptible to Lipid Peroxidation. *J. Phys. Chem. B* **2004**, *108*, 7170−7179.
(24) Hess, B.; Kutzner, C.; van der Spoel, D.; Lindahl, E. GROMACS 4: Algorithms for Highly Efficient, Load-Balanced, and Scalable Molecular Simulation. *J. Chem. Theory Comput.* **2008**, *4*, 435−447.
(25) Pronk, S.; Pall, S.; Schulz, R.; Larsson, P.; Bjelkmar, P.; Apostolov, R.; Shirts, M. R.; Smith, J. C.; Kasson, P. M.; van der Spoel, D.; Hess, B.; Lindahl, E. GROMACS 4.5: A High-Throughput and Highly Parallel Open Source Molecular Simulation Toolkit. *Bioinformatics* **2013**, *29*, 845−854.
(26) Wong-Ekkabut, J.; Miettinen, M. S.; Dias, C.; Karttunen, M. Static Charges Cannot Drive a Continuous Flow of Water Molecules through a Carbon Nanotube. *Nat. Nanotechnol.* **2010**, *5*, 555−557.
(27) Wong-ekkabut, J.; Karttunen, M. Assessment of Common Simulation Protocols for Simulations of Nanopores, Membrane Proteins, and Channels. *J. Chem. Theory Comput.* **2012**, *8*, 2905−2911.
(28) Essmann, U.; Perera, L.; Berkowitz, M. L.; Darden, T.; Lee, H.; Pedersen, L. G. A Smooth Particle Mesh Ewald Method. *J. Chem. Phys.* **1995**, *103*, 8577−8593.
(29) Hess, B.; Bekker, H.; Berendsen, H. J. C.; Fraaije, J. G. E. M. LINCS: A Linear Constraint Solver for Molecular Simulations. *J. Comput. Chem.* **1997**, *18*, 1463−1472.
(30) Bussi, G.; Donadio, D.; Parrinello, M. Canonical Sampling through Velocity Rescaling. *J. Chem. Phys.* **2007**, *126*, 014101.
(31) Berendsen, H. J. C.; Postma, J. P. M.; Vangunsteren, W. F.; Dinola, A.; Haak, J. R. Molecular-Dynamics with Coupling to an External Bath. *J. Chem. Phys.* **1984**, *81*, 3684−3690.
(32) Humphrey, W.; Dalke, A.; Schulten, K. VMD: Visual Molecular Dynamics. *J. Mol. Graphics* **1996**, *14*, 33−38.
(33) Weber, G.; Charitat, T.; Baptista, M. S.; Uchoa, A. F.; Pavani, C.; Junqueira, H. C.; Guo, Y. C.; Baulin, V. A.; Itri, R.; Marques, C. M.; Schroder, A. P. Lipid Oxidation Induces Structural Changes in Biomimetic Membranes. *Soft Matter* **2014**, *10*, 4241−4247.
(34) Kucerka, N.; Perlmutter, J. D.; Pan, J.; Tristram-Nagle, S.; Katsaras, J.; Sachs, J. N. The Effect of Cholesterol on Short- and Long-Chain Monounsaturated Lipid Bilayers as Determined by Molecular Dynamics Simulations and X-ray Scattering. *Biophys. J.* **2008**, *95*, 2792−2805.
(35) Vernier, P. T.; Levine, Z. A.; Wu, Y. H.; Joubert, V.; Ziegler, M. J.; Mir, L. M.; Tieleman, D. P. Electroporating Fields Target Oxidatively Damaged Areas in the Cell Membrane. *PLoS One* **2009**, *4*, e7966.
(36) Smith, H. L.; Howland, M. C.; Szmodis, A. W.; Li, Q. J.; Daemen, L. L.; Parikh, A. N.; Majewski, J. Early Stages of Oxidative Stress-Induced Membrane Permeabilization: A Neutron Reflectometry Study. *J. Am. Chem. Soc.* **2009**, *131*, 3631−3638.
(37) Mason, R. P.; Walter, M. F.; Mason, P. E. Effect of Oxidative Stress on Membrane Structure: Small-Angle X-ray Diffraction Analysis. *Free Radical Biol. Med.* **1997**, *23*, 419−425.
(38) Sabatini, K.; Mattila, J. P.; Megli, F. M.; Kinnunen, P. K. J. Characterization of Two Oxidatively Modified Phospholipids in Mixed Monolayers with DPPC. *Biophys. J.* **2006**, *90*, 4488−4499.
(39) Israelachvili, J. N.; Mitchell, D. J.; Ninham, B. W. Theory of Self-Assembly of Hydrocarbon Amphiphiles into Micelles and Bilayers. *J. Chem. Soc., Faraday Trans. 2* **1976**, *72*, 1525−1568.


DOI: 10.1021/acs.jpclett.5b02405
*J. Phys. Chem. Lett.* 2015, 6, 4884−4888